

Article

Class E Power Amplifier Design and Optimization for the Capacitive Coupled Wireless Power Transfer System in Biomedical Implants

Narayanamoorthi R. ¹ , Vimala Juliet A. ², Bharatiraja Chokkalingam ¹ ,
Sanjeevikumar Padmanaban ^{3,*}  and Zbigniew M. Leonowicz ⁴ 

¹ Department of Electrical and Electronics Engineering, SRM University, Chennai 603 203, India; narayanamoorthi.r@gmail.com (N.R.); bharatiraja@gmail.com (B.C.)

² Department of Electronics and Instrumentation Engineering, SRM University, Chennai 603 203, India; vimlala@yahoo.co.in

³ Department of Electrical and Electronics Engineering, University of Johannesburg, Auckland Park 2006, South Africa

⁴ Department of Electrical Engineering, Wrocław University of Science and Technology, Politechnika Wroclawska | Wyb. Wyspianskiego 27, 50-370 Wrocław, Poland; zbigniew.leonowicz@pwr.edu.pl

* Correspondence: sanjeevi_12@yahoo.co.in; Tel.: +27-79-219-9845

Received: 23 July 2017; Accepted: 31 August 2017; Published: 15 September 2017

Abstract: The capacitive coupled wireless power transfer (CCWPT) operating at megahertz (MHz) frequency is broadly considered as the promising solution for low power biomedical implants. The class E power amplifier is attractive in MHz range wireless power transfer (WPT) applications due to zero voltage switching (ZVS) and zero voltage derivative switching (ZVDS) properties. The existing design of class E amplifier is investigated only for inductive resonant coupled (IRC) WPT systems; the modelling and optimization of the class E amplifier for CCWPT systems are not deliberated with load variation. Meanwhile, the variations in the coupling distance and load are common in real time applications, which could reduce the power amplifier (PA) efficiency. The purpose of this paper is to model and optimize the class E amplifier for CCWPT systems used in MHz range applications. The analytical model of PA parameters and efficiency are derived to determine the optimal operating conditions. Also, an inductive-capacitive-inductive (LCL) impedance matching network is designed for the robust operation of the PA, which improves the efficiency and maintains required impedance compression. The maximum efficiency of the proposed design reached up to 96.34% at 13.56 MHz and the experimental results are closely matched with the simulation.

Keywords: capacitive coupled power transfer; class E amplifier; LCL compensation; biomedical implants

1. Introduction

WPT technology has been widely studied in different applications like electric vehicle charging, consumer electronics charging, radio-frequency identification (RFID) devices, bio implantable devices, and many more [1,2]. WPT techniques are broadly classified into near field and far field power transfer methods. Near field IRC and near field capacitive coupling methods are primarily investigated in the above mentioned applications [3,4]. Much research work has addressed the usage of near field IRC in biomedical implants and also some of the implants like pacemaker; chronic implants are available on the market with inductive powering technologies [5,6]. Even though the IRC method is well studied and established with standards, it has its own set of confinements, like requirements of rigid coil structure, less frequency bandwidth, and distributed electromagnetic fields on the tissue. In order to overcome these confinements of IRC, recently, the CCWPT system was analysed and tested in human

cadaver [7]. The electromagnetic interference and specific absorption rate in the CCWPT system is less than the IRC scheme in low range applications [8,9]. However, the power transfer efficiency of the system decays as the distance between the plates increases. In biomedical applications, the WPT system should be light weight, more efficient, and robust to changing load conditions [10]. In order to satisfy the above requirements, optimizing the WPT module alone is not sufficient; an improvement in each part of the system can increase the efficiency of the overall system. The overall efficiency of the CCWPT depends on the power source, the coupling capacitor plates, and the receiver circuit unit. The power source unit plays an important role in the CCWPT system after the capacitor plates module for the improvement of overall efficiency, which can increase the lifetime of the battery-driven implants. The WPT system in biomedical applications is normally operated under the MHz range of frequency to maintain the non-radiative characteristic of the electric and magnetic fields [11]. In [12], the switching PA topologies from class A to class E were discussed and recommended; the class E amplifier gives the highest efficiency with a lower number of switching devices in the MHz range. The class E amplifier is normally operated under ZVS and ZVDS conditions, which gives theoretically 100% efficiency [13]. However, the attainable efficiency of the class E amplifier is over 90% when the operating frequency and power level is of few MHz and tens of Watts, respectively [14]. Also, the class E amplifier design and modelling were extensively examined for the IRC WPT systems [15,16]. Since the performance of PA is sensitive to load variation under ZVS, ZVDS conditions and the efficiency drops drastically when there is variation in the designed optimum load value, which is the main concern in the WPT systems [17]. Different techniques are adopted to operate the class E amplifier in optimum conditions by tuning duty ratio, frequency, inductors, and capacitors [18,19]. Meanwhile, the class E amplifier with shunt capacitive compensation, inductive capacitive (LC) compensation, voltage Mode/current Mode control, loading, and power control techniques are discussed to compensate the variation in load impedance and coil coupling for IRC WPT systems [20,21]. For the high frequency and large bandwidth operation of PA, some modified structures are developed to meet the load variations [22–25]. However, these modified PA are realized with a complicated circuit design and control method, also intended for the specific applications. The study of class E PA for 50% duty cycle was performed for the IRC system with different load conditions [26]. The modelling and optimal parameters design of PA with IRC was discussed for biomedical applications [27,28]. However, to the authors' knowledge, the analysis and design of the class E amplifier for CCWPT systems have not been investigated extensively. The design of the CCWPT system with half and full bridge inverters is discussed for high power applications [29]. Also, the impedance matching circuits are designed to mitigate the coupling capacitor variation and load variations. The compensation of coupling capacitor variation using the series-resonant inductor was found to be a simple and effective method [30]. On the other hand, series inductance could not boost the voltage in the transmitter (Tx) side; also, the voltage pressure on the capacitance is high. To boost the voltage at the Tx side, LC compensation topology is utilized, but this method cannot provide required impedance compression when the load and the coupling capacitance change simultaneously [31]. Even though the impedance matching circuit is essential to mitigate the variations in the load impedance, it restricts the operating bandwidth of the PA. It gives better performance for constant frequency applications with static or dynamic load variations. Based on the above discussion, this paper attempts to design and optimize a class E amplifier for the CCWPT system used in low power biomedical applications. The analytical model of the PA is developed to obtain the optimal parameters for the different duty ratio. Also, to boost the voltage at the Tx plates and to attain the impedance compensation, an extra inductance is added along with the LC compensation circuit to get the 'T' shape LCL matching network. The addition of inductance provides the ability to suppress the effects of variation in coupling capacitance and load resistance. Figure 1 shows the diagram of the proposed class E amplifier with the CCWPT system used in biomedical applications.

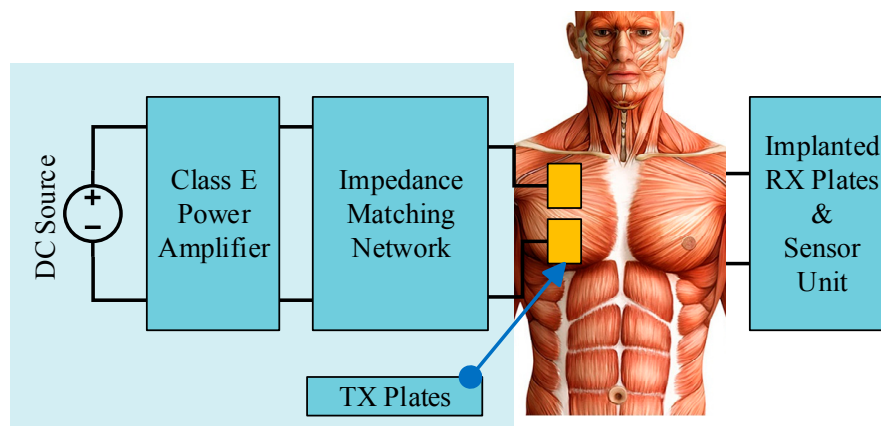


Figure 1. The diagram of capacitive coupled wireless power transfer (CCWPT) system in bio implants.

2. Capacitive Coupled WPT

The CCWPT schematic diagram is shown in Figure 2a. It uses the displacement current to transfer the energy between the transmitter and receiver plates without any conducting medium. The simple CCWPT circuit is formed with two pairs of conducting plates: supply unit and load. The power transfer capacity of the system depends on the effective capacitance formed between two plates and the operating frequency.

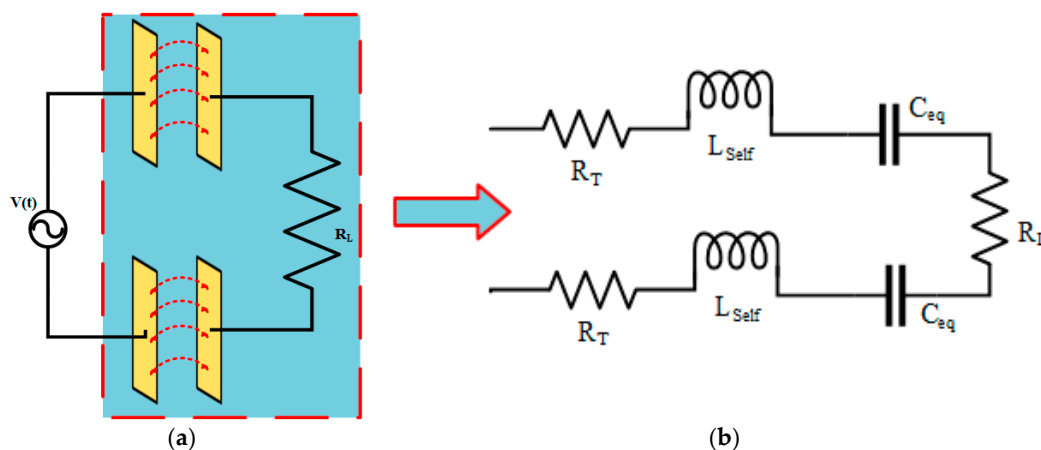


Figure 2. (a) Schematic diagram of CCWPT; (b) equivalent circuit of CCWPT.

The conduction current (I_c) and displacement current (I_d) between the plates are

$$I_c = \frac{V(t)\sigma A}{D} \quad (1)$$

$$I_d = \varepsilon_0 \varepsilon_r A \frac{dE}{dt} \quad (2)$$

where σ , A , D , ε_0 , ε_r , E are conductivity of the medium, the area of the plate, the distance between the plates, free space and relative permittivity, and the electric field strength, respectively. In order to increase the power transfer, the displacement current needs to be increased and the conduction current has to be minimized to reduce the power loss in the tissue. This can be obtained by considering the optimum values of A , E , D , and ε_r . For the theoretical analysis of the CCWPT system, the equivalent circuit model allows us to determine an optimal tradeoff between different loss and source power. Nevertheless, the tissue properties directly related with its characteristics like thickness and fat content

will vary from person to person. The conductor loss due to ohmic resistance and plate resistance in the CCWPT system are much smaller than the tissue loss under the MHz operating frequency range. However, for the precise modelling, the conductor loss resistance is considered in series with the tissue resistance to determine the equivalent resistance. Hence, the CCWPT module equivalent circuit can be modeled by considering the equivalent resistance (R_T), lead wires, and plate self-inductance (L_{self}), as well as the equivalent capacitance between the plates (C_{eq}) [7]. The equivalent circuit model of the CCWPT module is shown in Figure 2b.

3. Class E Amplifier with CCWPT

Figure 3 shows the class E power amplifier circuit diagram with CCWPT. It consists of the DC power source (V_{dc}), the Feed choke inductor (L_{FC}), the metal-oxide-semiconductor field-effect transistor (MOSFET) switch (SW), the shunt capacitance (C_P), the resonant circuit inductance (L_S), the capacitance (C_S), and the capacitive coupling equivalent circuit.

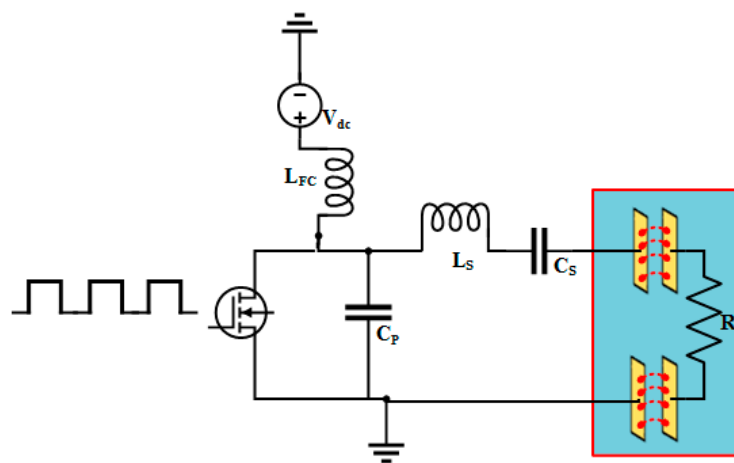


Figure 3. Class E power amplifier with CCWPT module.

The optimal values of circuit parameters can be derived by considering the following permissible assumptions:

- (1) The L_{FC} should be large enough to restrict the alternating current return to the direct current (DC) power supply.
- (2) The load quality factor (Q_L) is high enough to maintain the load current as pure sinusoidal.
- (3) The switching device has zero ON and OFF state loss.
- (4) Parasitic resistance values of all the parameters are neglected.

The power amplifier operating at ZVS and ZVDS conditions are given as

$$v(\omega t)|_{\omega t=2\pi} = 0 \quad (3)$$

$$\dot{v}(\omega t)|_{\omega t=2\pi} = 0 \quad (4)$$

where $v(\omega t)$ is the voltage across the switch and the CCWPT circuit is considered as load impedance to the PA, which can be expressed as

$$Z_L = R_T + L_{self} + C_{eq} + R_L \quad (5)$$

Based on the assumption that the load current $i_Z(\omega t)$ that appears across the Z_L will be sinusoidal in nature

$$i_Z(\omega t) = I_Z \sin(\omega t + \varphi) \quad (6)$$

where φ , I_Z are initial phase shift and load fundamental current amplitude, respectively. Allow the switch to be ON during the first half period, i.e., $\omega t = (0, 2\pi\delta)$, where δ is the duty ratio. The voltage across the switch is

$$v(\omega t) = V_{dc} - v_L(\omega t) - v_Z(\omega t) = 0 \quad (7)$$

The voltage across the inductor ($v_L(\omega t)$) and voltage across the load ($v_Z(\omega t)$) are

$$v_L(\omega t) = \omega L \frac{di_L(\omega t)}{d\omega t} \quad (8)$$

$$v_Z(\omega t) = V_Z \sin(\omega t - \varphi) \quad (9)$$

The current flowing through the switch $i(\omega t)$ and the shunt capacitance $i_C(\omega t)$ are

$$i_C(\omega t) = \omega C \frac{dv(\omega t)}{d\omega t} = 0 \quad (10)$$

$$i(\omega t) = i_L(\omega t) = \frac{1}{\omega L} \int_0^{2\pi\delta} v_L(\omega t) d\omega t \quad (11)$$

$$i_L(\omega t) = \frac{1}{\omega L} \int_0^{2\pi\delta} (V_{dc} + V_Z \sin(\omega t - \varphi)) d\omega t + i_L(0) \quad (12)$$

The initial value of the current in the inductor at $\omega t = 0$ is $i_L(0) = 0$, then from (12)

$$i_L(0) = -\frac{V_Z}{\omega L} \cos \varphi \quad (13)$$

Substituting (13) for (12), the current flowing through the switch during the ON state is

$$i(\omega t) = \frac{2\pi\delta V_{dc}}{\omega L} + \frac{V_Z}{\omega L} [\cos(2\pi\delta + \varphi) - \cos \varphi] \quad (14)$$

Considering from $2\pi\delta < \omega t \leq 2\pi$, the switch is turned off, the current flowing through the switch is $i(\omega t) = 0$, and the shunt capacitor current is same as the current in L_{FC}

$$i_C(\omega t) = \omega C \frac{dv(\omega t)}{d\omega t} \quad (15)$$

$$i_C(\omega t) = \frac{1}{\omega L} \int_{2\pi\delta}^{2\pi} (V_{dc} - v(\omega t) - V_Z \sin(\omega t + \varphi)) d\omega t + i_L(2\pi\delta) \quad (16)$$

The linear nonhomogeneous differential form of the above equation is

$$\omega^2 LC \ddot{v}(\omega t) + v(\omega t) - V_{dc} + V_Z \sin(\omega t + \varphi) = 0 \quad (17)$$

The general solution of the second order differential Equation (17) in normalized form is

$$\frac{v(\omega t)}{V_{dc}} = A_1 \cos\left(\frac{\omega t}{\omega\sqrt{LC}}\right) + A_2 \sin\left(\frac{\omega t}{\omega\sqrt{LC}}\right) + 1 + \frac{V_Z \sin(\omega t + \varphi)}{V_{dc}(\omega^2 LC - 1)} \quad (18)$$

The initial conditions are applied at $\omega t = 2\pi\delta$ to determine that the coefficients A_1 and A_2 are given by

$$A_1 = \frac{V_Z}{V_{dc}} \left[\left(1 + \frac{Q}{1-Q^2}\right) \cos(2\pi\delta + \varphi) \sin(2Q\pi\delta) - \frac{Q^2}{1-Q^2} \cos(2\pi Q\delta) \sin(2\pi\delta + \varphi) \right] - 2\pi\delta Q \sin(2\pi\delta Q) - \cos(2\pi\delta Q) \quad (19)$$

$$A_2 = \frac{V_Z}{V_{dc}} \left[\left(1 - \frac{Q}{1-Q^2}\right) \cos(2\pi\delta + \varphi) \cos(2Q\pi\delta) - \frac{Q^2}{1-Q^2} \sin(2\pi Q\delta) \sin(2\pi\delta + \varphi) \right] + 2\pi\delta Q \cos(2\pi\delta Q) - \sin(2\pi\delta Q) \quad (20)$$

Since the class E amplifier does not have any power consuming elements, then, theoretically, the efficiency of the amplifier for any duty cycle is 100%. The output power can be written as

$$P_0 = \frac{V_z^2}{2Z} = \frac{2V_{dc}^2 \sin^2(2\pi\delta) \sin(2\pi\delta + \varphi)}{\pi^2(1 - \delta)^2 Z} \quad (21)$$

From Equation (18) the average dc current is given as

$$I_{dc} = \frac{1}{2\pi\omega L} \left\{ 2\pi^2\delta^2 V_{DD} - 2\pi\delta V_z \cos(\varphi) + V_z [\sin(2\pi\delta + \varphi) - \sin(\varphi)] \right\} \quad (22)$$

From Equation (18), (21), and (22) the shunt capacitor, load impedance, series resonant inductor, and capacitor can be expressed as the function of V_{dc} and P_0

$$C_p = \frac{P_0(1 - \delta) \cos(2\pi\delta + \varphi) [\pi(1 - \delta) \cos(2\pi\delta) + \sin(2\pi\delta)]}{\omega V_{dc}^2 \sin(2\pi\delta + \varphi) \sin(2\pi\delta)} \quad (23)$$

$$Z = \frac{2V_{dc}^2 \sin^2(2\pi\delta) \sin^2(2\pi\delta + \varphi)}{\pi^2(1 - \delta)^2 P_0} \quad (24)$$

$$L_s = \frac{V_{DD}^2}{2\pi\omega P_0} \left\{ 2\pi^2\delta^2 - 2\pi\delta V_z \cos(\varphi) + V_z [\sin(2\pi\delta + \varphi) - \sin(\varphi)] \right\} \quad (25)$$

$$C_s = \frac{1}{\omega L_s} \quad (26)$$

The applied input power can be expressed as the sum of output power and loss

$$P_{in} = P_0 + P_{loss} \quad (27)$$

Switching loss due to the ON state resistance (R_{ds}) in the circuit is

$$P_{lsw} = \int_0^{2\pi\delta} i(\omega t)^2 R_{ds} d\omega t \quad (28)$$

$$P_{lsw} = \left(\frac{P_0}{V_{dc}} \right)^2 \left[2 - \delta + \frac{\pi(1 - \delta)^2 [2\pi\delta - \cos(2\pi\delta + 2\varphi) \sin(2\pi\delta)]}{(\cos(2\pi\delta + \varphi) - \cos(\varphi))^2} \right] R_{ds} \quad (29)$$

The total loss (P_{loss}) in the circuit is the sum of switching loss (P_{lsw}), ESR loss of shunt capacitance (P_{lcp}), choke inductance loss (P_{lch}), resonant series inductance loss (P_{lrl}), and capacitance loss (P_{lrc}). The efficiency of the power amplifier is given by

$$\eta = \frac{P_0}{P_0 + P_{lsw} + P_{lcp} + P_{lrl} + P_{lrc} + P_{lch}} \quad (30)$$

Since the parasitic resistance of all the elements are assumed to be negligible, the power losses P_{lcp} , P_{lch} , P_{lrl} , P_{lrc} are not considered in the efficiency calculation. The maximum voltage stress across the switch occurs at the zero voltage slope i.e., $\frac{dv(\omega t)}{d\omega t} = 0$ from $2\pi\delta$ to 2π , and maximum current stress occurs during the period 0 to $2\pi\delta$. From (18) and (14), the maximum voltage V_{smx} and current I_{smx} stress are given by

$$V_{smx} = \frac{V_{dc} \sin(\pi\delta) \tan(\pi\delta + \varphi)}{(1 - \delta)(\sin(\pi\delta) + \pi(1 - \delta) \cos(\pi\delta))} \left[\omega t - 2\pi\delta + \frac{2\pi(1 - \delta)(\cos(\omega t + \varphi) - \cos(2\pi\delta + \varphi))}{\cos(2\pi\delta + \varphi) - \cos(\varphi)} \right] \quad (31)$$

$$I_{smx} = I_{dc} \left[1 - \frac{2\pi(1 - \delta) \sin(\omega t + \varphi)}{\cos(2\pi\delta + \varphi) - \cos(\varphi)} \right] \quad (32)$$

The independent parameters V_N , φ , Q , P_0 , and P_{loss} are expressed in terms of duty ratio δ . The optimal selection of the duty ratio, considering the circuit element values, is the most important task for improving the amplifier efficiency.

4. Parameter Optimization and Model Verification

In the class E amplifier powered WPT system design the frequency f , load resistance R_L , required output power P_0 , and load current I_Z are known parameters. Duty ratio δ and shunt capacitance C_p are the input parameters required to calculate the unknown parameters from Equations (23)–(25). It is necessary to consider two constraints while finding the optimized design parameters. Primarily, the amplifier efficiency must be as high as possible to improve the overall efficiency, thereby a reduction in the CCWPT size and the switching voltage should be below the threshold limit to protect the switch from breakdown.

4.1. Optimal Parameters Selection

The duty ratio decides the conduction period of the MOSFET, which normally affects the switching loss and the efficiency of the amplifier. The circuit parameters for the different duty ratio values are numerically calculated from Equations (23)–(25) and are shown in Table 1. In a practical scenario, all the circuit elements must have positive values. If some circuit elements are not realizable, then the adjacent value of the duty ratio can be selected. Table 2 shows the other PA parameters considered for the design.

Table 1. Class E amplifier parameters for different duty ratio with CCWPT.

ffi	0.10	0.15	0.20	0.25	0.30	0.35	0.40	0.45	0.50
L_s (μH)	−0.561	−0.142	0.0342	0.162	0.246	0.452	0.571	0.892	0.943
C_s (nF)	−0.257	−0.231	−0.131	0.0921	0.1531	0.1714	0.1932	0.2001	0.2011
φ	−1.734°	−16.34°	−23.74°	−27.14°	−34.40°	−39.71°	−41.4°	−44.12°	−47.73°
Q	0.928	1.131	1.142	1.341	1.453	1.521	1.614	1.642	1.723
V_N	0.295	0.410	0.5856	0.6808	0.760	0.8712	0.91664	0.9516	0.9568
R_L (Ω)	7.032	7.634	8.043	9.764	11.023	12.103	12.984	13.541	15.031
X (p Ω)	−0.321	−0.231	0.132	0.234	0.312	0.388	0.401	0.441	0.561

Table 2. Class E amplifier parameters.

Parameters	Values
f (MHz)	13.56
P_0 (W)	5
C_p (pF)	176
L_{FC} (mH)	10
V_{dc} (V)	12

For different values of duty ratio, the efficiency and the conduction angle of the amplifier are plotted as shown in Figure 4. The maximum value of the efficiency can reach up to 96.34% for the duty ratio 0.45 and, when δ raises from 0.45 to 1, the PA efficiency reduces from 96.34% to 81.11% and, correspondingly, the conduction angle increases. The decrease in the efficiency from 0.5 to 1 is due to the increase in the conduction loss of the switch (P_{sw}), and the nominal voltage across the load raises to a maximum value at 0.45 duty ratio, as shown in Figure 5. During the ON period, the current through the switch is maximum and the voltage across the switch is zero. In the OFF period the voltage across the switch is high and the current through the switch is zero. So, the maximum current stress occurs for the duty ratio of 0.1 to 0.5 (ON condition) and the maximum voltage stress occurs for the duty ratio of 0.5 to 1 (OFF condition), as shown in Figure 6. The minimum power loss or switching loss occurs at 0.4 to 0.45 duty ratio, as given in Figure 7.

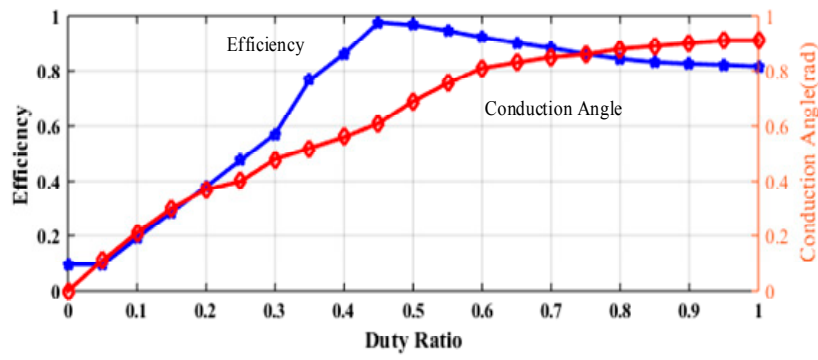


Figure 4. PA efficiency versus duty ratio.

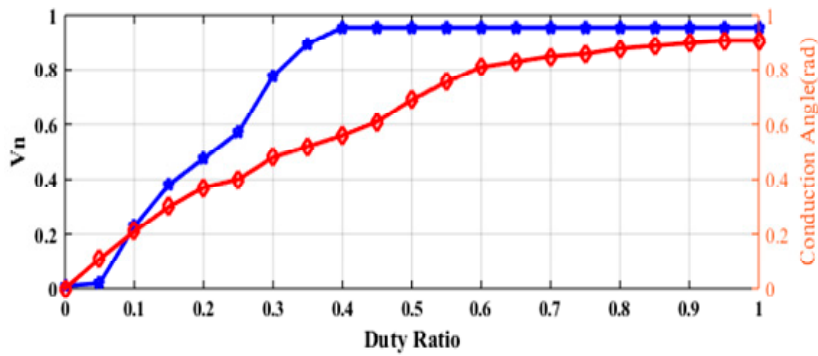


Figure 5. PA normalized voltage, angle versus duty ratio.

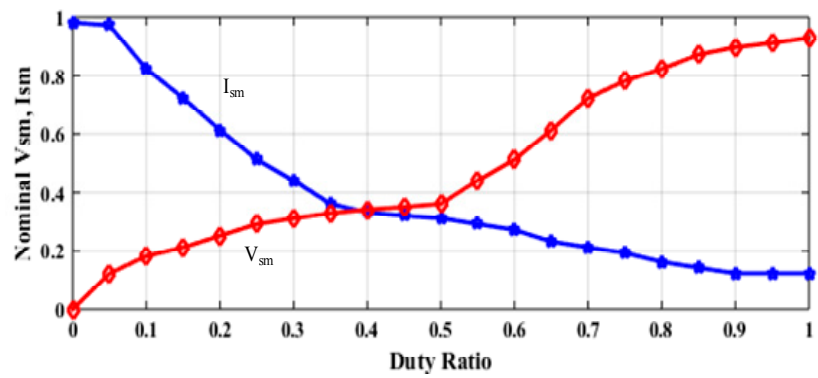


Figure 6. PA nominal V_{smx} , I_{smx} versus duty ratio.

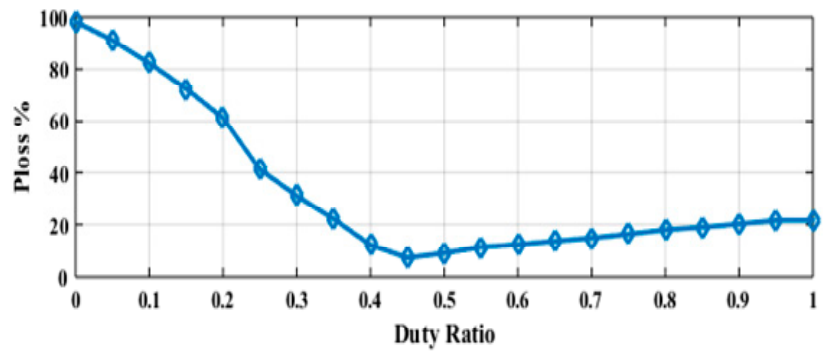


Figure 7. PA power loss versus duty ratio.

4.2. Simulation Verification

Based on the above analytical verification, the circuit parameters are chosen from the Tables 1 and 2 at 0.45 duty ratio. The class E amplifier with the capacitive coupling equivalent circuit is simulated in Advanced Design System (ADS) software for a different duty ratio, as shown in Figure 8. The voltage across the load, the switch voltage, and the current agree with the theoretical analysis of the ZVS and ZDS conditions. For the simulation, the parasitic resistance values of shunt capacitance and resonant circuit inductance and capacitance are not considered. As the duty ratio is reduced, glitches in the switch current are increased due to the discharge current from the shunt capacitor and the voltage drop across the switch being reduced. The switch voltage drop (V_{sw}) for the duty ratio of 0.45 is 1.3 V, whereas for the duty ratio of 0.2 it is reduced to 500 mV. The load voltage and current for the duty ratio of 0.45 are shown in Figure 8e,f respectively.

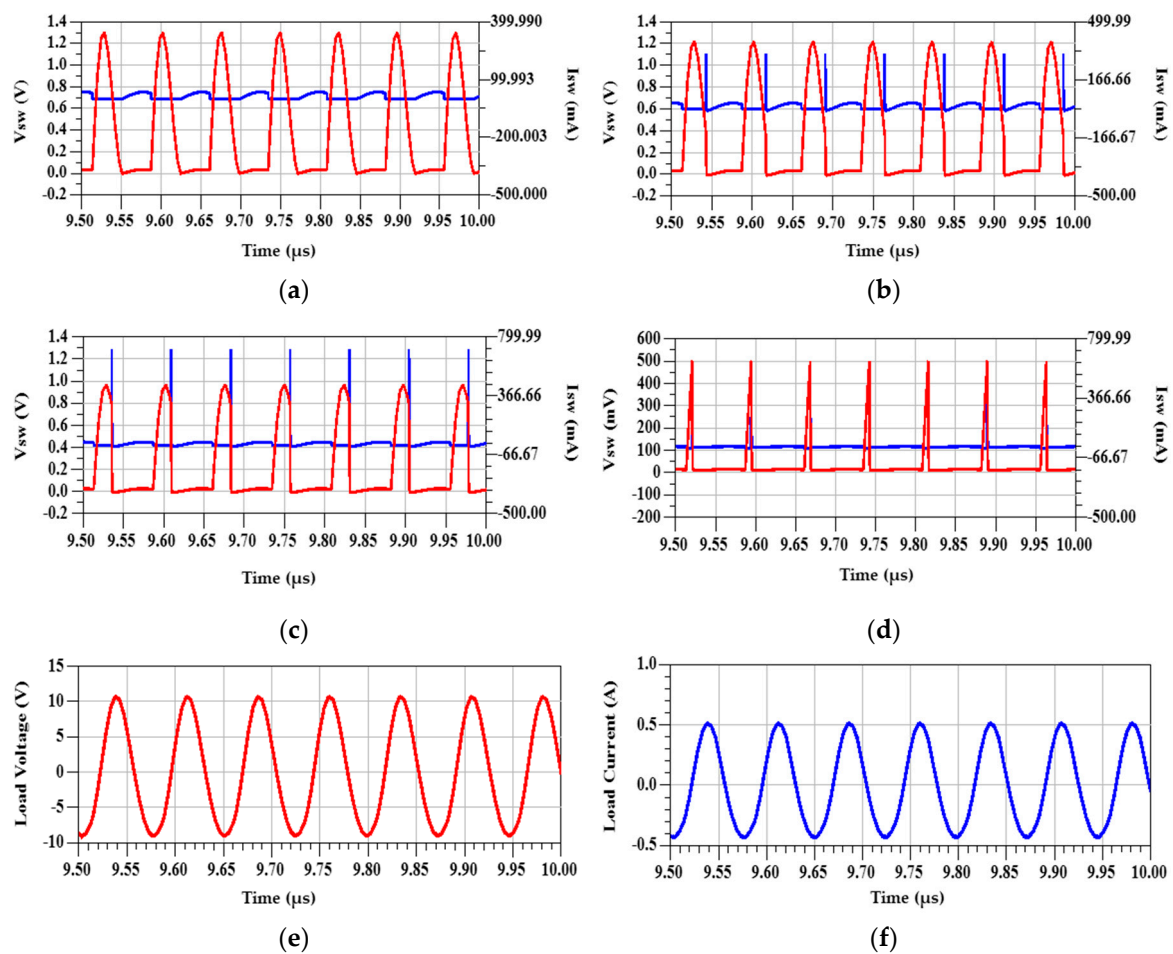


Figure 8. Switching voltage (red line) and current (blue line) of PA for different duty ratios: (a) $\delta = 0.45$; (b) $\delta = 0.4$; (c) $\delta = 0.3$; (d) $\delta = 0.2$; (e) load voltage at $\delta = 0.45$; and (f) load current at $\delta = 0.45$.

4.3. Capacitive Coupling Variation

In the CCWPT system, the size and shape of the plates varies based on the application requirements. The effective capacitance formed between the transmitter (Tx) and receiver (Rx) plates is in the order of a few tens to hundreds of pF. In some of the biomedical devices like capsule endoscope robots, the position of the receiver plates is not constant due to the continuous movement of the robots. The increase in the coupling distance reduces the effective capacitance value formed between the plates and thereby causes a reduction in the load voltage. The sudden variation in the coupling introduces the spikes in the switching voltage and current which could damage the MOSFET. Figure 9 shows the

MOSFET voltage, current, and load voltage for the variation of effective capacitance from 0.4 pF, 0.3 pF, and 0.1 pF. At 0.4 pF the designed voltage occurs in the load side and with a further reduction in the effective capacitance value to 0.1 pF, the load voltage is reduced to 3 V. The variation in the coupling distance also causes the impedance matching problem in the PA, which causes the reduction in the maximum power received by the load and the efficiency of the amplifier.

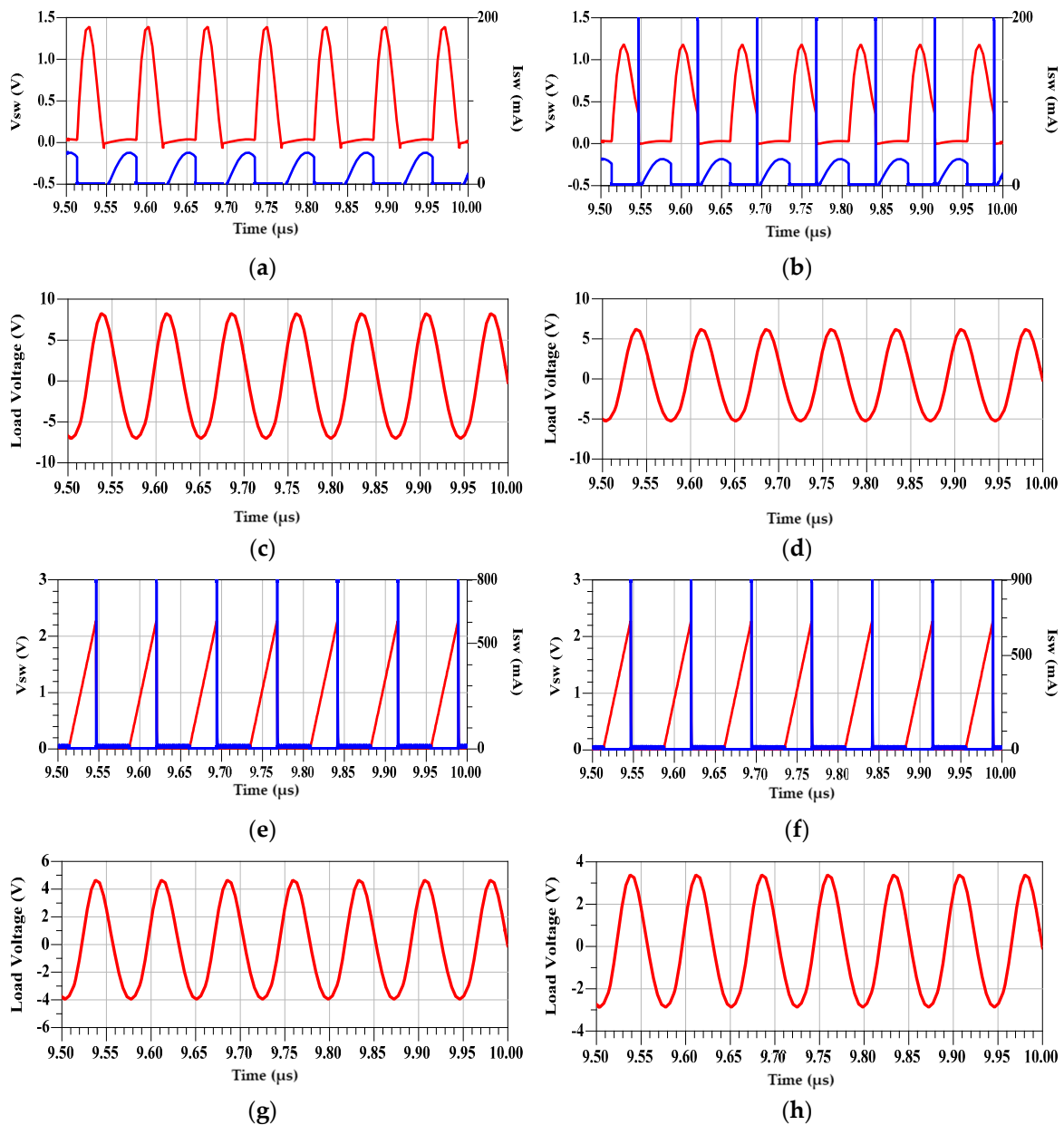


Figure 9. Switch voltage (red line) and current (blue line) of PA for different coupling capacitances: (a) V_{sw} and I_{sw} at $C_{eq} = 0.4$ pF; (b) V_{sw} and I_{sw} at $C_{eq} = 0.3$ pF; (c) Load Voltage at $C_{eq} = 0.4$ pF; (d) load voltage at $C_{eq} = 0.3$ pF; (e) V_{sw} and I_{sw} at $C_{eq} = 0.2$ pF; (f) V_{sw} and I_{sw} at $C_{eq} = 0.1$ pF; (g) Load Voltage at $C_{eq} = 0.2$ pF; and (h) Load Voltage at $C_{eq} = 0.1$ pF.

4.4. Load Variation

It is known that the soft switching conditions of the amplifier can be obtained when $R_L = R_{opt}$. The variation in load causes the deviation in the ZVS condition of class E PA. Figure 10 shows the performance of the PA under different load conditions. The switch voltage and current spikes are

increased during the ON and OFF state as the R_L values are changed from 13.5Ω , 16Ω , and 21Ω , as shown in Figure 10. The power dissipation (P_{diss}) across the MOSFET is raised from 10 mW to 100 mW and load power is reduced from 5 W to 3.1 W, which can significantly reduce the efficiency of class E PA. The glitches in the switch voltage and current are mainly due to the variation in the duty ratio and the load resistance, as well as the coupling between the plates. The variation on these parameters causes the discharge current from the shunt capacitor to flow through the switch, which increases the glitches in the switch current.

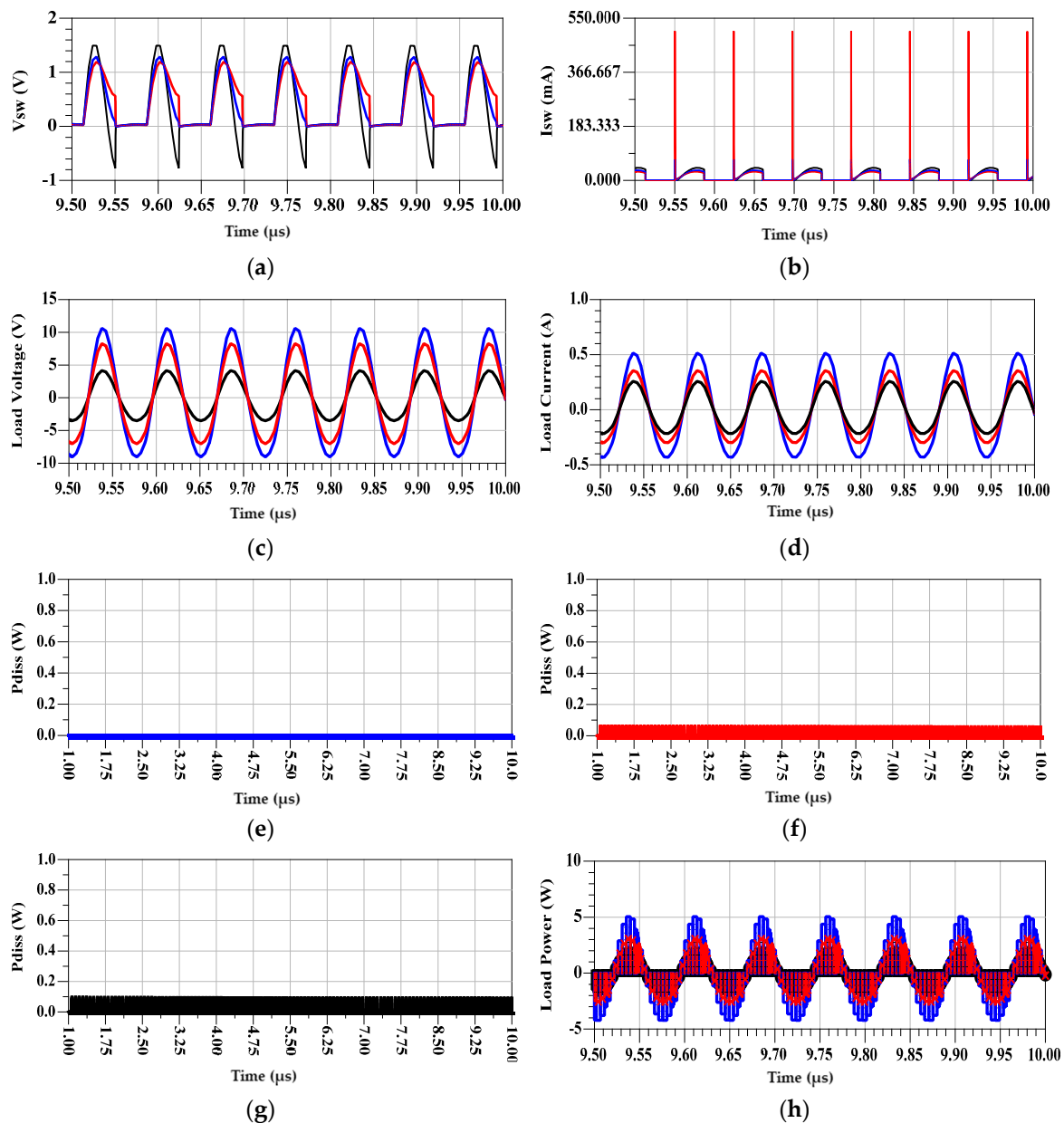


Figure 10. PA load variation (blue line) $R_L = 13.5 \Omega$, (red line) $R_L = 16 \Omega$, (black line) $R_L = 21 \Omega$: (a) V_{sw} ; (b) I_{sw} ; (c) load voltage; (d) load current; (e) power dissipation across switch at $R_L = 13.56 \Omega$; (f) power dissipation across switch at $R_L = 16 \Omega$; (g) power dissipation across switch at $R_L = 21 \Omega$; and (h) load power.

4.5. Impedance Matching

A further improvement in PA efficiency under the variations in load and coupling capacitance can be achieved by adding the impedance matching network. Figure 11a shows the LCL circuit model with the class E CCWPT circuit and Figure 11b gives the equivalent circuit model of the LC and LCL compensation network. At first, the frequency response of PA with the LC matching circuit is measured and compared with the LCL matching response; the reflection coefficient gain error in LC is of -12 dB and less than -1 dB in the LCL circuit at 13.56 MHz, as shown in Figure 12. For further analysis, the LCL network is considered and the parameters of the network can be obtained by finding the source (Z_1) and load (Z_2) impedance for the matching network [30].

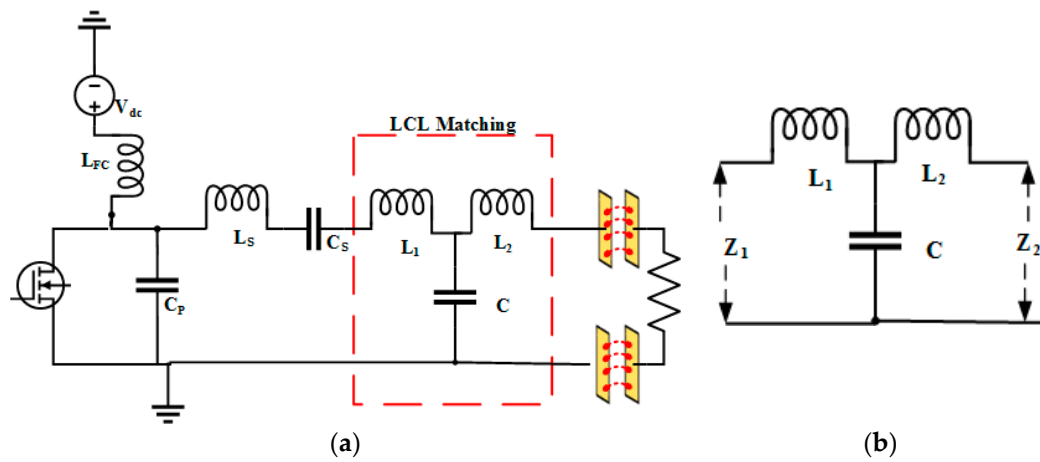


Figure 11. (a) Class E PA with LCL matching circuit; (b) T network model.

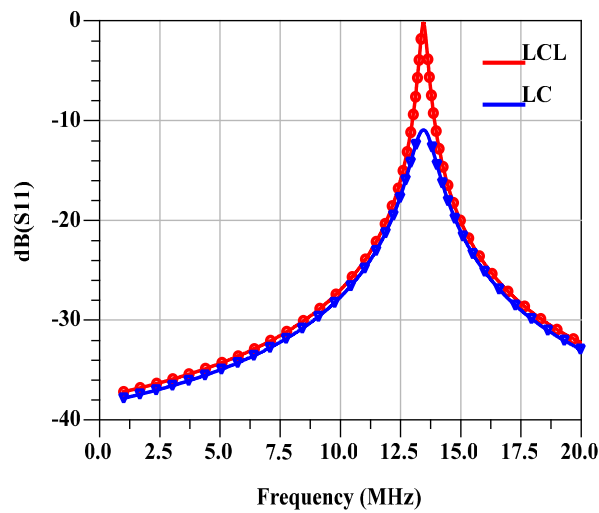


Figure 12. Frequency response of PA with matching.

For the LC matching circuit the L_1 and C_1 are

$$L_1 = \frac{Z_1 Q_1}{\omega_0}; L_2 = \frac{Z_2 Q_2}{\omega_0} \tag{33}$$

$$C = \frac{2Q_0}{\omega_0 Z_1 (1 + Q_1^2)} = \frac{2Q_0}{\omega_0 Z_2 (1 + Q_2^2)} \tag{34}$$

$$Q_1 = \frac{2Q_0 - \sqrt{4kQ_0^2 - (k-1)^2}}{1-k}; Q_2 = \frac{2kQ_0 - \sqrt{4kQ_0^2 - (k-1)^2}}{k-1} \quad (35)$$

where Q_1 , Q_2 , Q_0 are the quality factor at the input, the output of T network, and the desired quality factor, respectively, and the variable $k = \frac{Z_1}{Z_2}$. With the desired Q_0 from Table 1 at $\delta = 0.45$, L_1 , C , and L_2 are estimated as 214 nH, 18.5 pF, and 214 nH, respectively.

Figure 13 shows that the output power and efficiency contours in the smith chart are increasing as the load resistance values are increased from 6 Ω to 15 Ω. The PA efficiency is improved with the LCL compensation network to 96.34% for the load variation from 13.5 Ω to 15 Ω, whereas, in case without the impedance matching circuit, the η gets reduced after the optimal load point, as shown in Figure 13a. Also the ZVS and ZCS conditions of the PA are maintained with very minimal loss in the switch. The V_{sw} , I_{sw} , and load voltage for the load resistances values of 13.5 Ω, 16 Ω, and 21 Ω are displayed in Figure 14b–d.

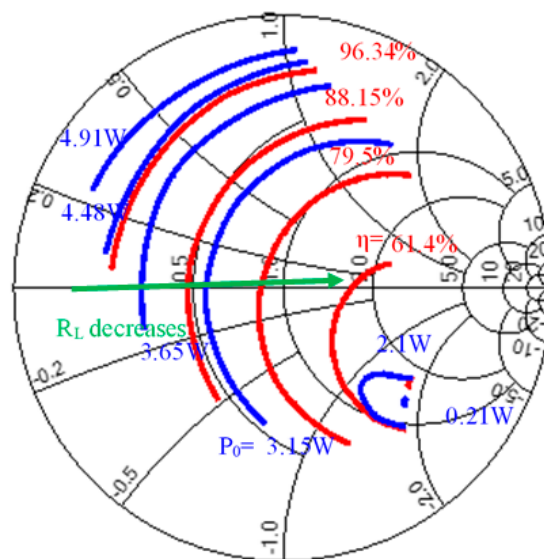


Figure 13. Variations of η and P_0 versus load.

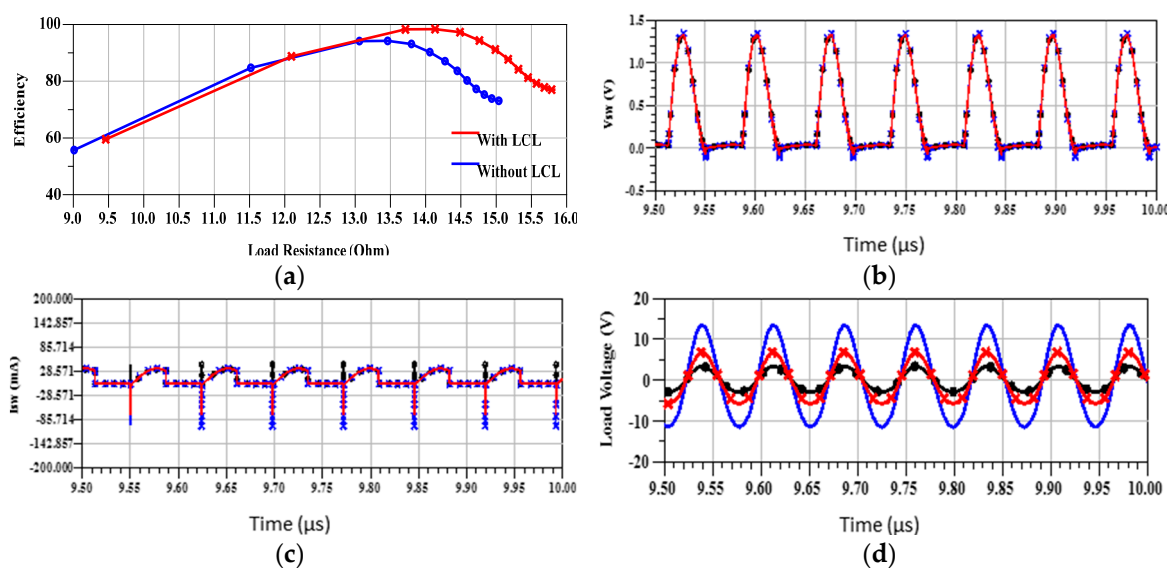


Figure 14. PA load variations variation $R_L = 13.5 \Omega$ (blue line), $R_L = 16 \Omega$ (red line), $R_L = 21 \Omega$ (black line): (a) η versus R_L ; (b) V_{sw} versus R_L ; (c) I_{sw} versus R_L and (d) load voltage.

4.6. Capacitance Modelling

The performance of CCWPT is studied by modelling three layers of human tissue consisting of skin, fat, and muscle in Comsol multiphysics software (5.2a, COMSOL Multiphysics Pvt. Ltd., Bengaluru, India). The dimensions, electrical conductivity (σ), dielectric constant (ϵ) of the tissue layers, and capacitive plates are given in Table 3 [26]. Figure 15 shows the schematic diagram of capacitive plates placement in the tissue model. The size of the Tx side plates are chosen to be more than the receiver plates to get better coupling. The 3D modelling of the designed CCWPT system is enclosed with the rectangular shape Gaussian surface and the Tx plates are connected with the cylindrical shape 0.1 mm radius contact wire to the external source. Similarly, the Rx plates are connected through 0.1 mm radius wire to the load circuit. The Tx plates are excited with the AC source of 10 V, 13.56 MHz, and the Rx plates are connected to the load resistance of 13.5 Ω . For meshing and analysis of the designed system, physics-controlled mesh is selected to get a fine mesh size and electric field physics in the frequency domain study is chosen for analysis. Two cases are considered in the simulation; initially, the Rx plates are placed under the muscle and, secondly, the Rx plates are placed under the skin. For the former case, the electric voltage distribution, Electric Normal Field distribution, Electric Displacement Field distribution, and current density in the model are shown in Figure 16. The Rx plate voltage is reached to 7.6 V with the separation of 40 mm and the electric field strength is of 0.45×10^3 V/m, which is much less than the maximum allowed value of 8.3×10^3 V/m for the frequency range of 3 kHz to 20 MHz [32]. The Electric displacement field and current density at the Rx plates are 1×10^{-8} to 2×10^{-8} C/m² and 1.5 A/m², respectively.

Table 3. Tissue layers dimensions and properties.

Layer	Length (mm)	Width (mm)	Depth (mm)	Electric Conductivity (S/m)	Dielectric Constant
Skin	15	30	4	0.6657	48.0980
Fat	45	30	4	0.0403	5.6000
Muscle	45	30	8	0.7834	57.5960
Tx Plates	15	20	1	5.998×10^7	1.12
Rx Plates	15	25	1	5.998×10^7	1.12

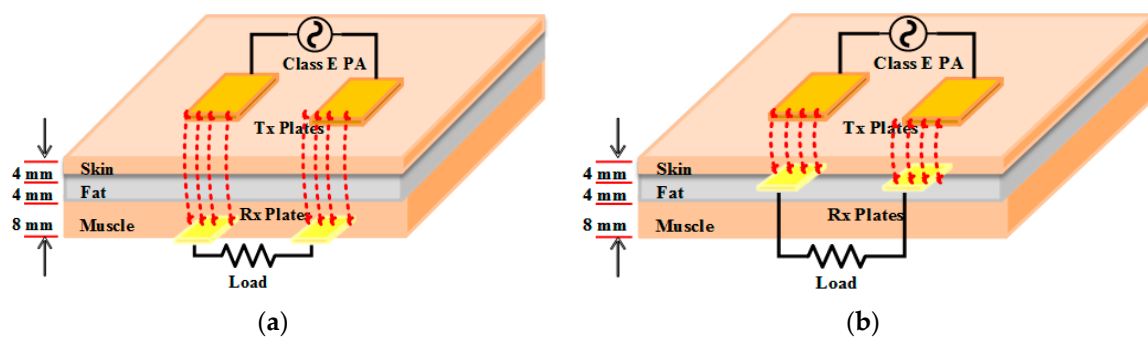


Figure 15. Schematic diagram of tissue with capacitive plates: (a) Rx plates under Muscle; and (b) Rx plates under skin.

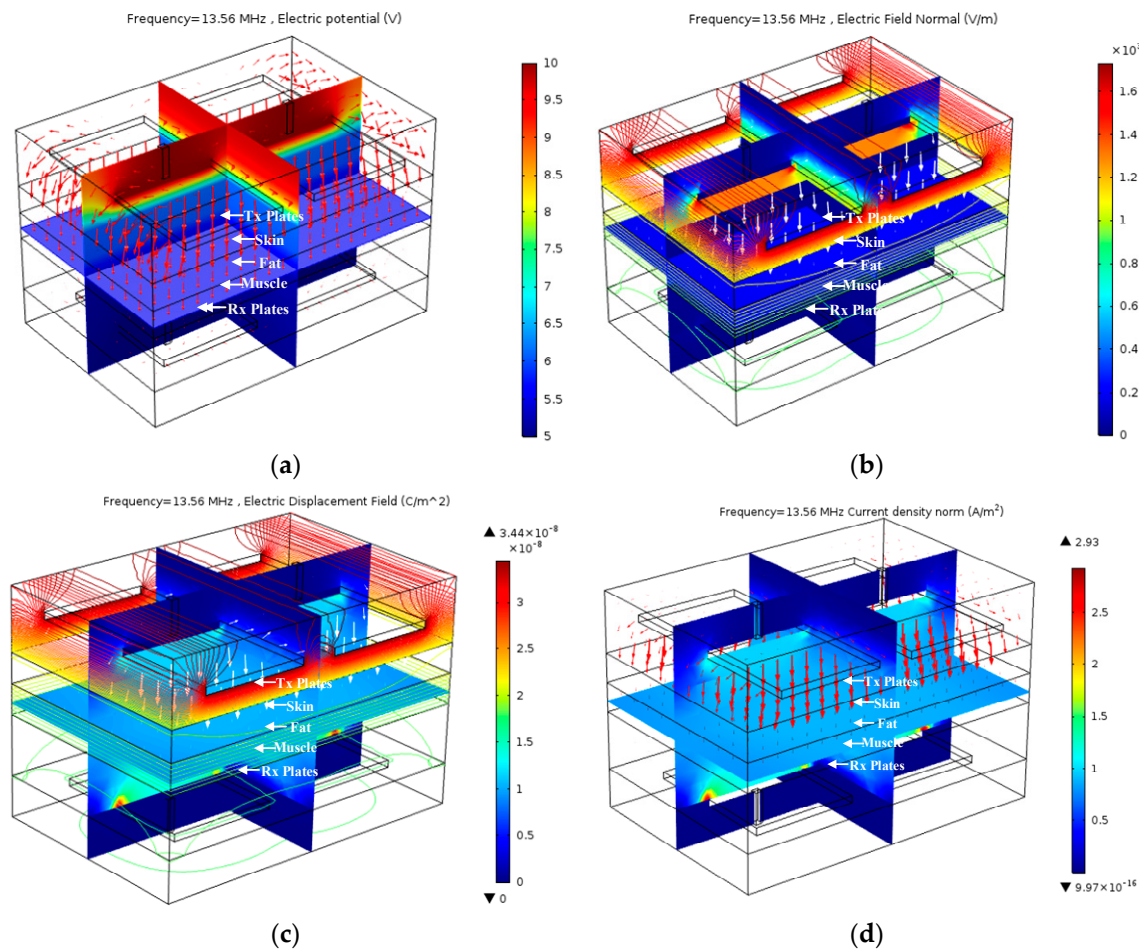


Figure 16. Finite element method (FEM) simulation of CCWPT by placing Rx plates under the muscle: (a) electric potential; (b) electric field normal; (c) electric displacement field; and (d) current density.

In the second case, the Rx plates are placed below the skin and above the fat layer, and the electric potential, field strength, displacement field, and current density at the Rx plates are 8.25 V, 0.57 V/m, 2.5×10^{-8} to 3×10^{-8} C/m², and 2.2 A/m², respectively. Even though the position of the Rx plates is changed from the bottom of the muscle to the top of the fat layer, there is not much increment observed in the Rx plates voltage. This is due to the properties of skin, which has a larger loss as compared to fat, bone, and muscle; the simulation results are shown in Figure 17. In both the cases, it is observed that the electric field and current density are within the safe limit as per the standards [32].

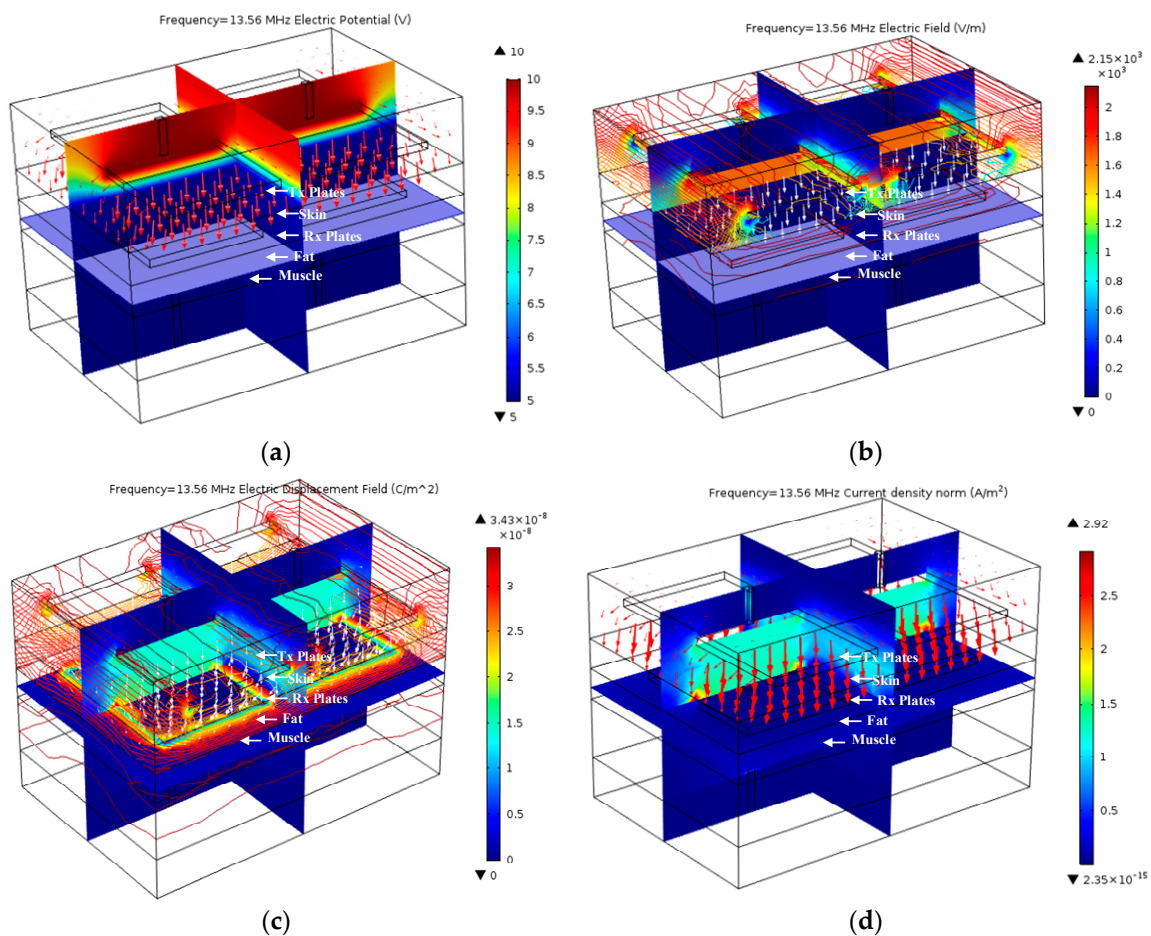


Figure 17. FEM simulation of CCWPT by placing Rx plates under the skin: (a) electric potential; (b) electric field normal; (c) electric displacement field; and (d) current density.

5. Experimental Analysis

To validate the performance of the proposed class E PA with the CCWPT system, the experimental setup has been designed as shown in Figure 18. The capacitor plates are made up of copper foil and encapsulated with a biocompatible polydimethylsiloxane layer and placed on acrylic board for support as shown in Figure 19. The Tx and Rx plates dimensions are same as the simulation dimension. In order to test the system with human tissue, a liquid solution is prepared mimicking the human tissue properties. The solution is prepared by following the IEEE standard for human tissue properties with $\epsilon_r = 46.741$ and $\sigma = 0.68892$ S/m at the ISM band using deionized water, salt, and sugar at a ratio of 56.18%, 41.49%, and 2.33% respectively [33]. The solution and capacitive plates are placed in a container made up of acrylic sheet with a dimension of 12 cm \times 12 cm \times 12 cm, as shown in Figure 18. The PA is designed with CSD13380F3 12-V N-Channel FemtoFET MOSFET (Texas Instruments (TI), Dallas, TX, USA), which have a low on-state resistance of 63 m Ω and a maximum gate to source voltage of 8 V. A high frequency driver of TPS28226 (Texas Instruments (TI)) is used as drive the MOSFET, and the National Instruments virtual bench VB-8014 (National Instruments, Bengaluru, India) is used as the signal generator to trigger the driver circuitry.

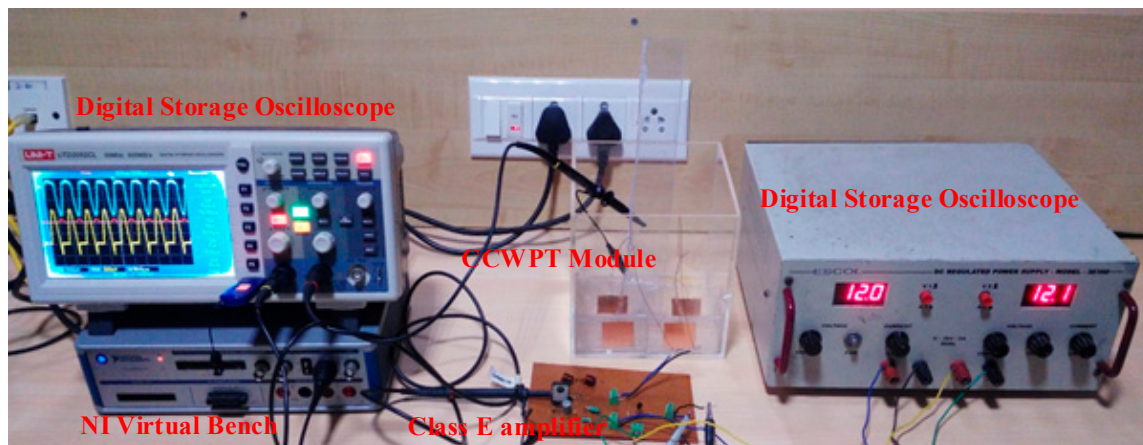


Figure 18. Experimental Setup of Class E PA with CCWPT.

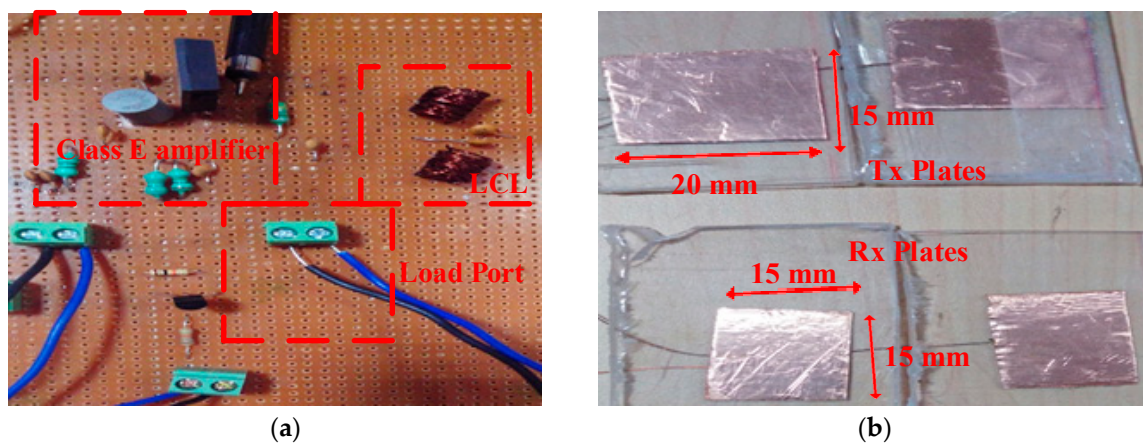


Figure 19. Designed PA circuit (a); class E PA board (b) Tx and Rx Plates.

The Rx plates are connected to the movable support and the load of variable resistance; initially, the distance between the plates is fixed at 40 mm and the optimal load resistance at 13.5Ω . The load voltage and switch voltage (V_{sw}) are shown in Figure 20a. The peak switch voltage in the MOSFET is 3.5 V, and the Rx plate voltage is 9.1 V with 14% glitches present in V_{sw} . When the load resistance values are increased to 21Ω by keeping the same distance between the plates, the V_{sw} is 2.1 V with 14% glitches during the ON condition and load voltage is reduced to 5 V, as shown in Figure 20b. Next, the distance between the plate capacitance is increased to 60 mm and $R_L = 13.5 \Omega$, and the glitches in V_{sw} are raised up to 18%, as given in Figure 20c. Figure 20d shows the V_{sw} and load voltage for the increase in R_L and the distance of 21Ω and 60 mm. In all, the cases of the voltage spikes in the MOSFET are less than the maximum allowed voltage of 8 V, and the ZVS conditions are achieved.

The load voltage and current are measured using the NI VB-8014 digital multimeter (National Instruments, Bengaluru, India) for different load conditions, and the output power is calculated. The maximum experimental efficiency of the proposed model reached 91.34%, and the deviation in the efficiency is because of the wire resistance and practical imperfection in the design of the inductor coil and capacitor plates. The comparison between the simulation and the experimental results is shown in Figure 21.

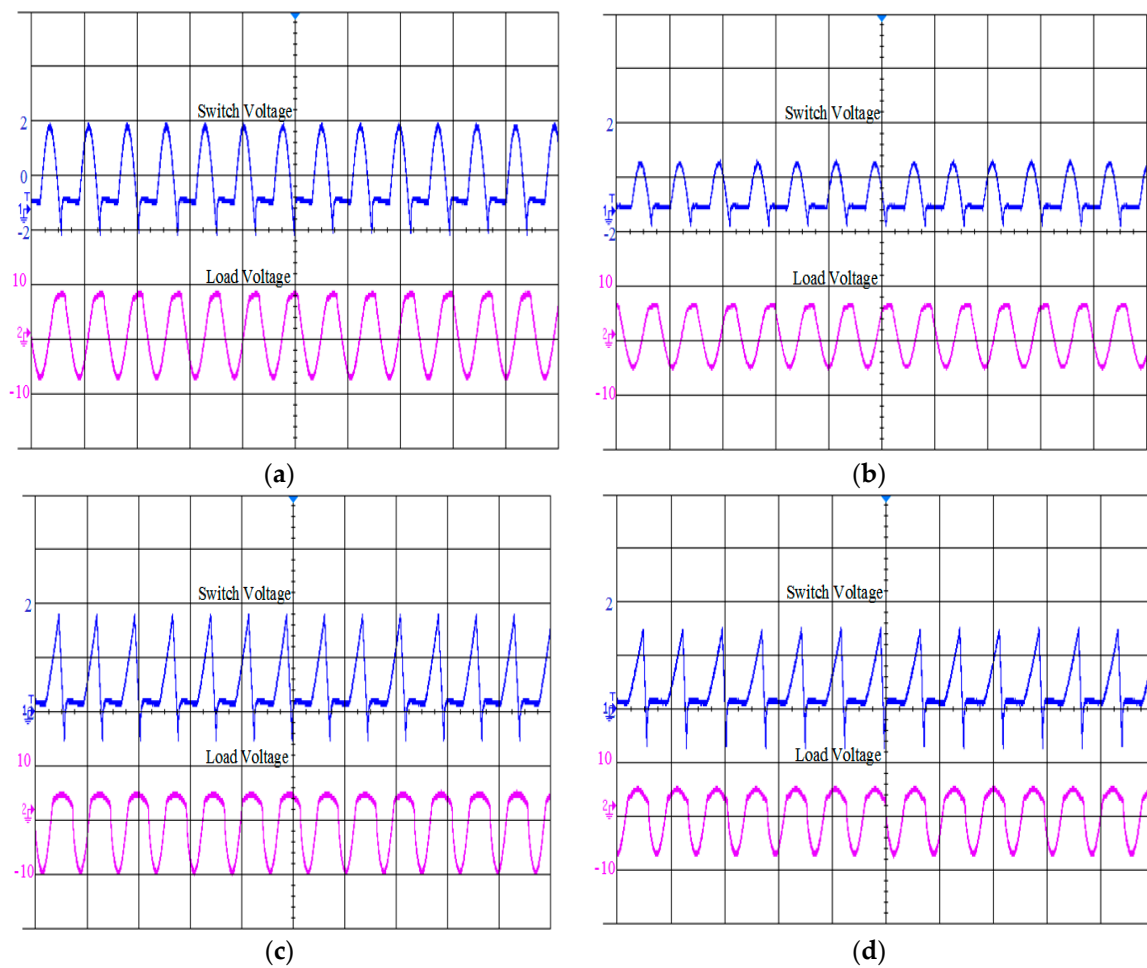


Figure 20. Experimental results of V_{sw} and load voltage: (a) $R_L = 13.5 \Omega$ at $d = 40$ mm; (b) $R_L = 21 \Omega$ at $d = 40$ mm; (c) $R_L = 13.5 \Omega$ at $d = 60$ mm; and (d) $R_L = 21 \Omega$ at $d = 60$ mm.

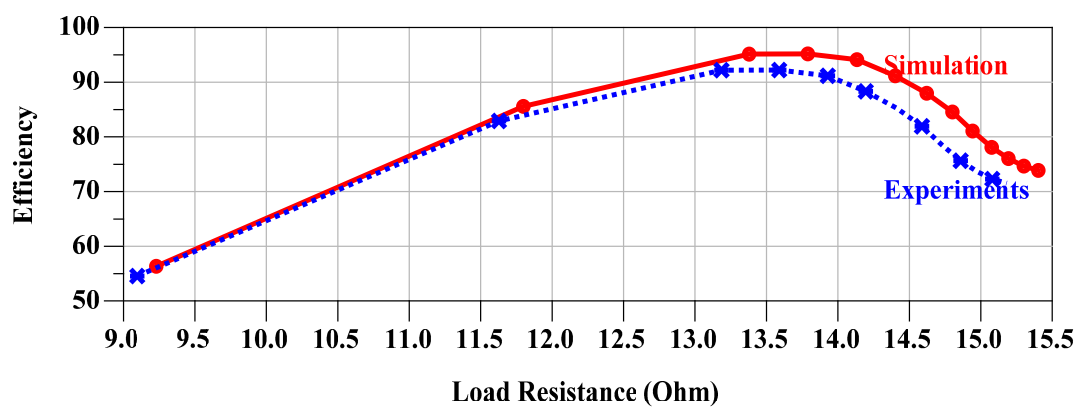


Figure 21. Comparison of simulated and experimental Efficiency.

6. Conclusions

The design of class E PA for CCWPT systems used in biomedical applications is discussed in this paper. The analytical model of the PA parameters is derived for a different duty ratio and the performance of the PA is analysed by selecting the optimal value of duty ratio. The effects of coupling capacitance variations and load variations are discussed with the optimal duty ratio and a LCL

impedance matching circuit is designed to improve the robustness of the PA. Also, the electric field distribution and current density in the human tissue model is studied using the FEM. Based on the simulation analysis, the efficiency of the class E PA with the CCWPT system gives 96.34% at 13.56 MHz, and the experimental results are close to the analytical results.

Author Contributions: All authors contributed equally for the research work and its final decision as article in its current form.

Conflicts of Interest: The authors declare no conflict of interest.

References

- Jawad, A.M.; Nordin, R.; Gharghan, S.K.; Jawad, H.M.; Ismail, M. Opportunities and Challenges for Near-Field Wireless Power Transfer: A Review. *Energies* **2017**, *10*, 1022. [[CrossRef](#)]
- Jiang, C.; Chau, K.T.; Liu, C.; Lee, C.H.T. An Overview of Resonant Circuits for Wireless Power Transfer. *Energies* **2017**, *10*, 894. [[CrossRef](#)]
- Li, X.; Meng, X.; Tsui, C.Y.; Ki, W.H. Reconfigurable Resonant Regulating Rectifier With Primary Equalization for Extended Coupling- and Loading-Range in Bio-Implant Wireless Power Transfer. *IEEE Trans. Biomed. Circuits Syst.* **2015**, *9*, 875–884. [[CrossRef](#)] [[PubMed](#)]
- Zhu, Q.; Wang, L.; Liao, C. Compensate Capacitor Optimization for Kilowatt-Level Magnetically Resonant Wireless Charging System. *IEEE Trans. Ind. Electron.* **2014**, *61*, 6758–6768. [[CrossRef](#)]
- Lu, Y.; Ma, D.B. Wireless Power Transfer System Architectures for Portable or Implantable Applications. *Energies* **2016**, *9*, 1087. [[CrossRef](#)]
- Xiao, C.; Liu, Y.; Cheng, D.; Wei, K. New Insight of Maximum Transferred Power by Matching Capacitance of a Wireless Power Transfer System. *Energies* **2017**, *10*, 688. [[CrossRef](#)]
- Jegadeesan, R.; Agarwal, K.; Guo, Y.X.; Yen, S.C.; Thakor, N.V. Wireless Power Delivery to Flexible Subcutaneous Implants Using Capacitive Coupling. *IEEE Trans. Microw. Theory Tech.* **2017**, *65*, 280–292. [[CrossRef](#)]
- Dai, J.; Ludois, D.C. A Survey of Wireless Power Transfer and a Critical Comparison of Inductive and Capacitive Coupling for Small Gap Applications. *IEEE Trans. Power Electron.* **2015**, *30*, 6017–6029. [[CrossRef](#)]
- Zhang, R.; Liu, H.; Shao, Q.; Li, G.; Fang, X.; Li, H. Effects of Wireless Power Transfer on Capacitive Coupling Human Body Communication. *IEEE/ASME Trans. Mechatron.* **2015**, *20*, 1440–1447. [[CrossRef](#)]
- Li, X.; Tang, C.; Dai, X.; Deng, P.; Su, Y. An Inductive and Capacitive Combined Parallel Transmission of Power and Data for Wireless Power Transfer Systems. *IEEE Trans. Power Electron.* **2017**, *PP*, 1. [[CrossRef](#)]
- Hsu, J.U.W.; Hu, A.P.; Swain, A. A Wireless Power Pickup Based on Directional Tuning Control of Magnetic Amplifier. *IEEE Trans. Ind. Electron.* **2009**, *56*, 2771–2781. [[CrossRef](#)]
- Wang, G.; Liu, W.; Sivaprakasam, M.; Kendir, G.A. Design and Analysis of an Adaptive Transcutaneous Power Telemetry for Biomedical Implants. *IEEE Trans. Circuits Syst. I* **2005**, *52*, 2109–2117. [[CrossRef](#)]
- Hannan, M.A.; Hussein, H.A.; Mutashar, S.; Samad, S.A.; Hussain, A. Automatic Frequency Controller for Power Amplifiers Used in Bio-Implanted Applications: Issues and Challenges. *Sensors* **2014**, *14*, 23843–23870. [[CrossRef](#)] [[PubMed](#)]
- Sokal, N.O.; Sokal, A.D. Class E-A New Class of High-efficiency Tuned Single-ended Switching Power Amplifiers. *IEEE J. Solid-State Circuits* **1975**, *SC-10*, 168–176. [[CrossRef](#)]
- Liu, H.; Shao, Q.; Fang, X. Modeling and Optimization of Class-E Amplifier at Subnominal Condition in a Wireless Power Transfer System for Biomedical Implants. *IEEE Trans. Biomed. Circuits Syst.* **2017**, *11*, 35–43. [[CrossRef](#)] [[PubMed](#)]
- Yang, T.; Liang, J.; Zhao, C.; Chen, D. Analysis and Design of class-E Power Amplifier at Any Duty in Frequency Domain. *Analog Integr. Circ. Sig. Process.* **2011**, *67*, 149–156. [[CrossRef](#)]
- Casanova, J.J.; Low, Z.N.; Lin, J. Design and Optimization of a Class-E Amplifier for a Loosely Coupled Planar Wireless Power System. *IEEE Trans. Circuits Syst. II* **2009**, *56*, 830–834. [[CrossRef](#)]
- Liu, M.; Zhao, C.; Song, J.; Ma, C. Battery Charging Profile-Based Parameter Design of a 6.78-MHz Class E² Wireless Charging System. *IEEE Trans. Ind. Electron.* **2017**, *64*, 6169–6178. [[CrossRef](#)]
- Liu, M.; Qiao, Y.; Liu, S.; Ma, C. Analysis and Design of A Robust Class E² DC–DC Converter for Megahertz Wireless Power Transfer. *IEEE Trans. Power Electron.* **2017**, *32*, 2835–2845. [[CrossRef](#)]

20. Liu, S.; Liu, M.; Fu, M.; Ma, C.; Zhu, X. A high-efficiency Class-E Power Amplifier with Wide-range Load in WPT Systems. In Proceedings of the 2015 IEEE Wireless Power Transfer Conference (WPTC), Boulder, CO, USA, 13–15 May 2015; pp. 1–3.
21. Fu, M.; Yin, H.; Liu, M.; Ma, C. Loading and Power Control for a High-Efficiency Class E PA-Driven Megahertz WPT System. *IEEE Trans. Ind. Electron.* **2016**, *63*, 6867–6876. [[CrossRef](#)]
22. Wilkinson, A.J.; Everard, J.K.A. Transmission-line Load-network Topology for Class-E Power Amplifiers. *IEEE Trans. Microw. Theory Tech.* **2001**, *49*, 1202–1210. [[CrossRef](#)]
23. Raab, F.H. Effect of Circuit Variations on the Class-E Tuned Power Amplifier. *IEEE J. Solid-State Circuits* **1978**, *SC-13*, 239–247. [[CrossRef](#)]
24. Moore, W.H.; Holschneider, D.P.; Givrad, T.K.; Maarek, J.I. Transcutaneous RF-powered Implantable Minipump Driven by a Class-E Transmitter. *IEEE Trans. Biomed. Eng.* **2006**, *53*, 1705–1708. [[CrossRef](#)] [[PubMed](#)]
25. Hayati, M.; Lotfi, A.; Kazimierzuk, M.K.; Sekiya, H. Analysis and Design of Class-E Power Amplifier with MOSFET Parasitic Linear and Nonlinear Capacitances at Any Duty Ratio. *IEEE Trans. Power Electron.* **2013**, *28*, 5222–5232. [[CrossRef](#)]
26. Fukui, K.; Koizumi, H. Class-E Rectifier with Controlled Shunt Capacitor. *IEEE Trans. Power Electron.* **2012**, *27*, 3704–3713. [[CrossRef](#)]
27. Rozario, D.; Pathipati, V.K.; Ram, A.; Azeez, N.A.; Williamson, S.S. Modified Resonant Converters for Contactless Capacitive Power Transfer Systems Used in EV Charging Applications. In Proceedings of the IECON 2016—42nd Annual Conference of the IEEE Industrial Electronics Society, Florence, Italy, 23–26 October 2016; pp. 4510–4517.
28. Sinha, S.; Kumar, A.; Pervaiz, S.; Regensburger, B.; Afridi, K.K. Design of Efficient Matching Networks for Capacitive Wireless Power Transfer Systems. In Proceedings of the 2016 IEEE 17th Workshop on Control and Modeling for Power Electronics (COMPEL), Trondheim, Norway, 27–30 June 2016; pp. 1–7.
29. Zhang, H.; Lu, F.; Hofmann, H.; Mi, C. An LC Compensated Electric Field Repeater for Long Distance Capacitive Power Transfer. In Proceedings of the 2016 IEEE Energy Conversion Congress and Exposition (ECCE), Milwaukee, WI, USA, 18–22 September 2016; pp. 1–5.
30. Chung, B.K. Q-based Design Method for T Network Impedance Matching. *Microelectron. J.* **2006**, *37*, 1007–1011. [[CrossRef](#)]
31. Gabriel, S.; Lau, R.W.; Gabriel, C. The Dielectric Properties of Biological Tissues: III. Parametric Models for the Dielectric Spectrum of Tissues. *Phys. Med. Biol.* **1996**, *41*, 2271–2293. [[PubMed](#)]
32. *IEEE Standard for Safety Levels With Respect to Human Exposure to Radio Frequency Electromagnetic Fields, 3 kHz to 300 GHz, IEEE Standard C95.1–2005*; IEEE: New York, NY, USA, 2006; pp. 1–238.
33. Challis, L.J. Mechanisms for Interaction between RF Fields and Biological Tissue. *Bioelectromagnetics* **2005**, *26*, S98–S106. [[CrossRef](#)] [[PubMed](#)]

